Journal of Colloid and Interface Science 346 (2010) 208–215

Contents lists available at ScienceDirect

Journal of Colloid and Interface Science

www.elsevier.com/locate/jcis

Determination of a setup correction function to obtain adsorption kinetic data at stagnation point flow conditions

Maria F. Mora [a,1], M. Reza Nejadnik [a,1], Javier L. Baylon-Cardiel [b], Carla E. Giacomelli [c], Carlos D. Garcia [a,*]

[a] Department of Chemistry, The University of Texas at San Antonio, United States
[b] Departamento de Ingeniería Eléctrica y Computacional, Tecnológico de Monterrey, Mexico
[c] INFIQC-Departamento de Fisicoquímica, Fac. de Ciencias Químicas, Universidad Nacional de Córdoba, Argentina

ARTICLE INFO

Article history:
Received 16 December 2009
Accepted 11 February 2010
Available online 13 February 2010

Keywords:
Spectroscopic ellipsometry
Stagnation point
Adsorption kinetics
Polyethylene glycol
Protein adsorption

ABSTRACT

This paper is the first report on the characterization of the hydrodynamic conditions in a flow cell designed to study adsorption processes by spectroscopic ellipsometry. The resulting cell enables combining the advantages of *in situ* spectroscopic ellipsometry with stagnation point flow conditions. An additional advantage is that the proposed cell features a fixed position of the "inlet tube" with respect to the substrate, thus facilitating the alignment of multiple substrates. Theoretical calculations were performed by computational fluid dynamics and compared with experimental data (adsorption kinetics) obtained for the adsorption of polyethylene glycol to silica under a variety of experimental conditions. Additionally, a simple methodology to correct experimental data for errors associated with the size of the measured spot and for variations of mass transfer in the vicinity of the stagnation point is herein introduced. The proposed correction method would allow researchers to reasonably estimate the adsorption kinetics at the stagnation point and quantitatively compare their results, even when using different experimental setups. The applicability of the proposed correction function was verified by evaluating the kinetics of protein adsorption under different experimental conditions.

Published by Elsevier Inc.

1. Introduction

The adsorption of macromolecules, colloids, and bioparticles to solid surfaces has been widely reported in the literature [1–5] with studies that include different methodologies, surfaces, and applications [6–8]. The time-dependent nature of the adsorption processes as well as the significance of their initial steps for various biomedical and industrial applications, highlight the importance of kinetic studies. Regardless of the selected analytical technique to follow the process, there are two main experimental approaches to study adsorption kinetics of particles: batch and flow experiments. Batch experiments are generally performed by monitoring the depletion of adsorbate in a dispersion of sorbent particles [9]. Although this approach is attractive due to its minimal instrumental requirements, it involves non-uniform hydrodynamic conditions, and is limited to slow adsorption processes. A more efficient way to study adsorption processes, particularly those involving shorter time-scales, is by flowing a solution of adsorbate over the sorbent surface. Several authors have pointed out the advantages of performing such studies including the well-controlled hydrodynamic conditions that allow accurate measurements, particularly regarding the initial stages of the adsorption/desorption phenomena [10,11]. Various flow displacement geometries have been used for such adsorption studies [12–15]. Among them, setups yielding stagnation point flow conditions are frequently used for measurement of adsorption kinetics [1,16–20]. Stagnation point flow conditions are obtained by perpendicularly impinging a jet of solution to the sorbent surface through a cylindrical channel. The stagnation point is defined as the intersection of the symmetry axis of the cylinder with the surface [1,21]. The main advantage of this arrangement is that the hydrodynamics of the mass flux at the stagnation point can be accurately described [1,22,23].

Stagnation point flow conditions have been used for adsorption studies in conjunction with several techniques such as microscopy [24], quartz crystal microgravimetry [20], evanescent wave light scattering [25], and reflectometry [8,20,22,26,27]. Our group is particularly interested in the application of spectroscopic ellipsometry (SE) for adsorption studies because it can provide real-time information regarding the kinetics of the adsorption process as well as the structure of the adsorbed layer for a broad range of materials and substrates. Ellipsometry is an optical technique that measures changes in the reflectance and phase difference between the parallel (R_P) and perpendicular (R_S) components of a polarized light beam upon reflection from a surface [28]. The intensity ratio of

* Corresponding author. Address: One UTSA Circle, San Antonio, TX 78249, USA. Fax: +1 210 458 7428.
E-mail address: carlos.garcia@utsa.edu (C.D. Garcia).
[1] Both authors contributed equally to this work.

0021-9797/$ - see front matter Published by Elsevier Inc.
doi:10.1016/j.jcis.2010.02.019

R_P and R_S can be related to the ellipsometric angles (Ψ, amplitude and Δ, phase difference as functions of wavelength or time) using Eq. (1):

$$\tan(\Psi)e^{i\Delta} = \frac{R_P}{R_S} \quad (1)$$

Spectroscopic ellipsometry allows the measurement of the ellipsometric angles as a function of the wavelength of the incident light beam. Because ellipsometry measures the ratio of two values originated by the same signal, the data collected are highly accurate and reproducible. The output values of ellipsometry are extremely sensitive to the thickness (down to the monolayer level), optical constants, and microstructure (such as surface roughness, index grading, and intermixing) of the films. This monolayer sensitivity is useful for real-time studies of film deposition, including the formation of layers of biological molecules on a wide variety of substrates [29–31]. It is worth noting that although dynamic adsorption studies performed by ellipsometry have been widely reported in the literature, the flow conditions in these reports have not been properly characterized [32–35]. In this regard, this paper provides the first fully characterized flow cell to perform ellipsometric adsorption studies under stagnation point flow conditions.

One common issue associated with the use of optical methods, such as reflectometry and ellipsometry, to perform adsorption kinetic studies is that these techniques typically underestimate the initial adsorption rate at the stagnation point [1,19,36]. The difference between the experimental and predicted values have been attributed to the fact that these instruments collect signals from a spot (few square millimeters) rather than an infinitesimal point (stagnation point) [19]. Therefore, the adsorption rates calculated based on these signals could be significantly smaller than the adsorption rates existing at the stagnation point. As a consequence, similar experiments performed with diverse experimental setups may render significantly different results (depending on the size of the measured area), making quantitative interlaboratory comparisons rather challenging.

Considering the aforementioned points, this paper is intended to address two important issues, it aims first, to demonstrate the advantages of combining ellipsometry with stagnation point flow conditions; and second, to provide a procedure to calculate a set-up-specific correction function that allows for correcting experimental kinetic data for errors associated with the size of the measured spot. In order to verify the consistency of obtained data in the proposed experimental setup with stagnation point flow conditions, the liquid cell used here was characterized by studying the adsorption kinetics of polyethylene glycol (PEG) to silica according to a procedure developed by Dijt et al. [1]. Then, theoretical calculations were performed by computational fluid dynamics and compared with the experimental data in order to determine the correction function needed for the geometry of our cell. Finally, the adsorption kinetics of two proteins were studied to demonstrate the applicability of the correction function to different analytes.

2. Materials and methods

2.1. Cell description

Dynamic adsorption experiments were performed in a commercial flow cell designed for spectroscopic ellipsometry (J.A. Woollam Co; Lincoln, NE). In order to control the flux of adsorbate to the substrate, the cell was modified by fixing an L-shaped stainless-steel tube ($R = 0.381$ mm) to the cell (see Fig. 1). One end of the tube faced the substrate at the same spot where the incident light beam hits the surface. The other end of the tube was connected, using Tygon tubing, to a peristaltic pump (Minipuls3, Gilson; Middleton, WI). A two-way valve (V100D, Upchurch Scientific; Oak Arbor, WA) was also connected in series to enable rapid switching between the background electrolyte and the solution containing the adsorbate. The distance from the end of the tube to the surface was kept constant ($h = 1.1$ mm) for experiments described herein. Using this arrangement, the adsorbate solution impinged the surface of the substrate with an angle of incidence equal to 90° (with respect to the surface). The proposed setup provides an alternative experimental design to those used by Arwin [33,37], Petri [38], Pérez [39], or Logothetidis [34] and enables monitoring of the adsorption process *in situ* and in real time. An additional advantage of the proposed modification is that the cell allows the adjustment of the distance between the inlet tube and the substrate providing versatility to the design (see Fig. 1). Furthermore, the fixed position

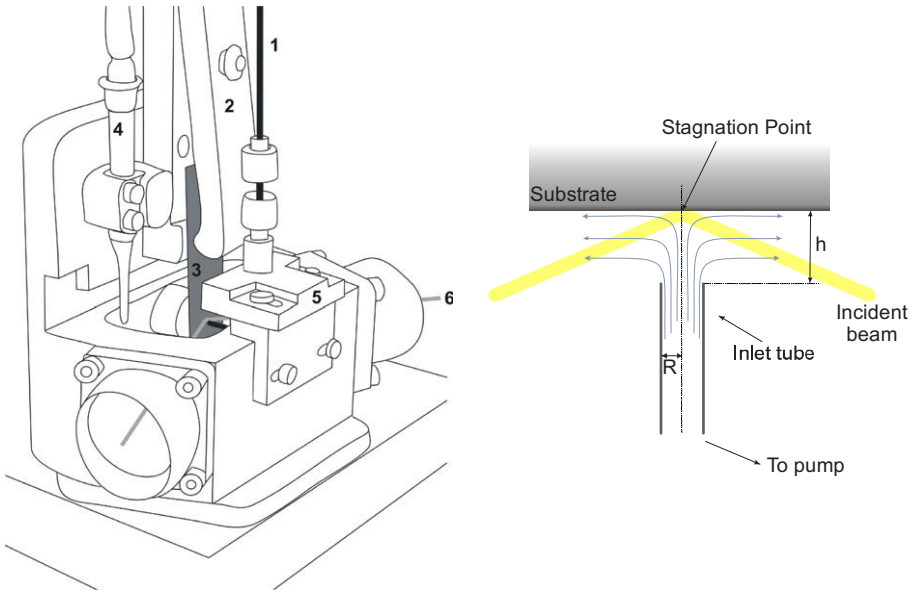

Fig. 1. Schematic drawing showing the described cell (left) and its main components: (1) inlet tube, (2) substrate holder, (3) substrate, (4) drain, (5) inlet tube positioner, and (6) incident beam. Top view of the cell (right), highlighting the arrangement of the tube with respect to the substrate (right).

of the inlet tube with respect to the substrate (which also has a fixed position) after adjustment, facilitates the alignment of different substrates.

2.2. Computational fluid dynamics

The cell was modeled using two parallel solid plates separated by a distance h. One of the plates was assigned to the substrate on which the adsorption process takes place, and used as a reference point (0, 0). The second plate (located at $z = h$) was assigned to the end of the L-shaped tube (of radius R), which delivers the solution containing the adsorbate. During all experiments described in this paper, the flow was developed in the cell, and the fluid moved to an outflow region, located away from the symmetry axis. For all the calculations, a ratio of h/R equal to 2.8 was considered and all the fluids were assumed to be Newtonian and incompressible. The ratio h/R is an important parameter that determines the flow distribution and the adsorption kinetics [40]. The flow of fluid along the cell can be characterized using the Reynolds number (Re), a dimensionless parameter defined as:

$$\mathrm{Re} = \frac{\rho R U}{\eta} \tag{2}$$

where ρ and η are the density and the viscosity of the fluid respectively, R is the radius of the tube, and U is the mean fluid velocity. The Reynolds number, which characterizes the tendency of a fluid to develop turbulence or to flow with a laminar regime, was varied in the 2–50 range. This range is significantly smaller than the value of Re at which the flow changes from laminar to turbulent (Re > 2000 [41,42]). Under the specified conditions, the laminar flow can be described using the steady-state Navier–Stokes equation and the continuity equation, as previously described by Dabros and van de Ven [10]. Due to the axisymmetrical design of the cell, these equations can be expressed in cylindrical coordinates r and z, with the form

$$-\frac{\partial p}{dr} + \eta\left(\frac{1}{r}\frac{\partial}{\partial r}\left(r\frac{\partial u_r}{\partial r}\right) - \frac{\partial^2 u_r}{\partial z^2} - \frac{u_r}{r^2}\right) = 0 \tag{3}$$

$$-\frac{\partial p}{dz} + \eta\left(\frac{1}{r}\frac{\partial}{\partial r}\left(r\frac{\partial u_z}{\partial r}\right) + \frac{\partial^2 u_z}{\partial z^2}\right) = 0 \tag{4}$$

$$\frac{1}{r}\frac{\partial}{\partial r}(r u_r) + \frac{\partial u_z}{\partial z} = 0 \tag{5}$$

where u_r is the radial component of the fluid velocity, p is the pressure, and u_z is the axial component of the fluid velocity. Coordinates were non-dimensionalized with respect to the radius R and the components of the fluid velocity were referred to the mean velocity U. The fluid flow at the exit of the tube was assumed to show a parabolic profile, accordingly with a developed Poiseuille flow. With this assumption, the boundary conditions required to solve Eqs. (3)–(5) can be formulated as:

$$u_r = u_z = 0 \quad \text{at the solid surfaces of the cell} \tag{6}$$

$$u_r = 0, u_z = U(1 - r^2) \quad \text{at the surface of the plate located at } z = 0 \tag{7}$$

$$\frac{\partial u_z}{\partial r} = 0 \quad \text{in the symmetry axis} \tag{8}$$

$$u_z = 0 \quad \text{at the outflow region of the cell} \tag{9}$$

The numerical solutions for the fluid flow equations were obtained using the finite element method, as implemented in the COMSOL Multiphysics software. A mesh consisting of 4000 quadrilateral elements and 4141 points was constructed along the geometry of the model cell. At each point, a solution was approximated with a low order polynomial, and was further refined through a number of iterations. Close to the surface of the plate located at $z = 0$, the radial and axial components of the fluid velocity can be approximated by the analytical expressions described in Eqs. (10) and (11),

$$u_r = \alpha r z \tag{10}$$

$$u_z = \alpha z^2 \tag{11}$$

where α is a dimensionless flow intensity parameter that is constant for a certain cell geometry and flow rate [43]. The proposed approach was validated by comparing the results obtained using different geometries [10]. In all cases, identical solutions were achieved.

2.3. Reagents and solutions

All chemicals were analytical reagent grade and used as received. All aqueous solutions were prepared using 18 MΩ cm water (NANOpure Diamond, Barnstead; Dubuque, Iowa). Monodisperse polyethylene glycol was purchased from Polymer Laboratories (Amherst, MA) and used without further purification. Stock solutions of PEG were prepared by dissolving a known amount of solid material in DI water. Catalase (CAT) from bovine liver was purchased as a lyophilized powder (2–5 Ug^{-1}) from Sigma Aldrich (Saint Louis, MO) and kept at −20 °C until used. Bovine serum albumin (BSA), fraction V (heat-shock treated) was purchased from Fisher scientific (Fair Lawn, NJ) and kept at −4 °C until used. Citrate buffer (10 mM) was selected as the background electrolyte because it provides high buffer capacity ($pKa_1 = 3.13$, $pKa_2 = 4.76$, $pKa_3 = 6.4$) around the isoelectric point (IEP) of the proteins ($IEP_{CAT} = 5.4$ [44] and $IEP_{BSA} = 4.7$ [45]). The pH of the solutions was adjusted using either 1 M NaOH or 1 M HCl (Fisher Scientific; Fair Lawn, NJ) and measured using a glass electrode and a digital pH meter (Orion 420A+, Thermo; Waltham, MA). Stock solutions of proteins were prepared by dissolving a known amount of protein in 10 mM citrate buffer. Other protein solutions were prepared by diluting the corresponding amount of stock in citrate buffer. Table 1 summarizes the corresponding molecular weights (M_w), ratio of weight to number molecular weight [46], and diffusion coefficients (calculated as described by Shao and Baltus [47]) of the selected polymers and proteins. All experiments were performed using ⟨1 1 1⟩ Si/SiO_2 wafers (Sumco; Phoenix, AZ) as substrates. Before each experiment, Si/SiO_2 substrates were cleaned in a 1:1 mixture of $HCl:H_2O_2$ for 10 min at 80 °C, rinsed thoroughly with water, and immersed in DI water until used to avoid contamination.

2.4. Adsorption experiments

Both the characterization of the substrates as well as the dynamic adsorption experiments were performed at room temperature using a variable angle spectroscopic ellipsometer (WVASE, J.A. Woollam Co; Lincoln, NE). Spectroscopic ellipsometry has proven suitable to study adsorption processes, and provides useful information about the optical constants and structure of the adsorbed film [37,48–51]. Dynamic adsorption experiments were

Table 1
Molecular weights, ratio of weight to number molecular weight, and calculated diffusion coefficients of PEG and the selected proteins.

	Molecular weight	M_W/M_N	D (10^{-7} cm^2 s^{-1})
PEG	278,100	1.05	1.36
PEG	93,000	1.06	2.50
PEG	8730	1.05	9.34
Catalase	250,000	–	4.00 [74]
Bovine serum albumin	66,000	–	5.93 [74]

Table 2
Optical parameters used to calculate the thicknesses and adsorbed amounts of the selected adsorbates. *A*, *B*, and *C* are the Cauchy parameters, *n* is the refractive index, and *dn*/*dc* is the variation of refractive index with concentration. The reported refractive indexes are the values obtained with the Cauchy parameters for 650 nm. The references included here reported the values of *n* for 633 nm.

	A	*B*	*C*	$n_{650\ nm}$	*dn*/*dc*
PEG	1.34	0.01	0	1.362 [1]	0.136 [1,56]
Proteins	1.44	0.01	0	1.465 [35]	0.180 [55,57]

performed in the modified cell which was mounted directly on the vertical base of the ellipsometer. In all experiments, the variation of Ψ and Δ as a function of time was determined at an angle of incidence of 70°, as defined by the inlet/outlet of the UV fused-silica windows. Considering that the adsorption of PEG onto silica is a rather fast process, only one wavelength (650 nm) was used in order to increase the data acquisition rate and to determine the initial adsorption rate ($(d\Gamma/dt)_{t\to 0}$) more accurately. The collected data were modeled using the WVASE software package (J.A. Woollam Co; Lincoln, NE). Experimental results were interpreted using a model consisting of three uniaxial layers with optical axes parallel to the substrate surface. The dielectric functions of the substrates were described by a layer of Si (bulk; $d = 1$ mm) and a layer of SiO_2 ($d = 2.5 \pm 0.5$ nm). The adsorbed layers were described using a Cauchy parameterization model, according to Eq. (12), where *A*, *B*, and *C* are computer-calculated fitting parameters, and λ is the wavelength of the incident light beam. The values of *A*, *B*, and *C* for each analyte were selected in such a way that the refractive indexes match the values reported in the literature [35]. The Cauchy constants as well as the refractive indexes are summarized in Table 2. In agreement with previous reports, the extinction coefficient of all the adsorbates used in this study was considered to be zero [1,52–54]. The mean square error (MSE) was used to quantify the difference between the experimental and model generated data.

$$n_{(\lambda)} = A + \frac{B}{\lambda^2} + \frac{C}{\lambda^4} \tag{12}$$

Prior to each adsorption experiment, a spectroscopic scan was performed for a clean strip of silicon wafer in order to determine the thickness of the SiO_2. This procedure allowed verifying the thickness of each substrate; therefore improving the accuracy of the calculation of the adsorbed layer. Then, the dynamic experiment was initiated by pumping water through the cell (~5 min) to measure the baseline. Next, the valve was switched, adsorbate solution was introduced, and the adsorption process started. After the process reached the corresponding equilibrium and no significant change in the signal was observed, the dynamic scan was stopped, and a more accurate spectroscopic scan was collected in the 300–850 nm range (with 10 nm steps). This scan was used to verify the thickness of the adsorbed layer.

The adsorbed amount (Γ, expressed in mg m^{-2}) was calculated using Eq. (13),

$$\Gamma = \frac{d(n - n_0)}{(dn/dc)} \tag{13}$$

where n and n_0 are the refractive index of the adsorbed layer (see Table 2) and the ambient (H_2O), respectively [55]. In accordance with previous reports [1,55–58], a constant refractive index increment (dn/dc) was considered for the adsorbed layers (see Table 2). Experiments performed in this way provided data for calculating the initial adsorption rate ($(d\Gamma/dt)_{t\to 0}$) and the saturation adsorbed amount (Γ_{SAT}). These values were calculated for the adsorption of PEG for different polymer concentrations, Reynolds numbers, and molecular weights, as well as for the adsorption of proteins.

2.5. Validation of experimental results

The rate of adsorption at the solid/liquid interface is generally considered to comprise three steps: transport of the solute molecules from the bulk to the interface, attachment to the surface, and relaxation on the surface. When perfect sink boundary conditions are present (concentration at the surface is zero) and in the absence of a barrier, the flux of solute (J) towards the surface can be described by Eq. (14),

$$J = 0.776 v^{1/3} R^{-1} (\alpha \mathrm{Re})^{1/3} D^{2/3} C \tag{14}$$

where v is the kinematic viscosity of the solvent, R the inner radius of the tube through which the solution enters the cell (0.381 mm), D the diffusion coefficient of the studied adsorbate and, C is the concentration of the solute in the bulk [1,59].

It is also worth considering that, depending on the interactions involved (van der Waals, electrostatic, polymer bridging, or steric repulsion), solutes have a certain probability of attaching to the surface. This probability is represented by the efficiency factor (β) which relates the flux of adsorbate (J) to the adsorption rate ($(d\Gamma/dt)_{t\to 0}$) according to Eq. (15). Other denominations commonly used in the literature to refer to this factor are retardation factor [43] or free surface area fraction [60].

$$\left(\frac{d\Gamma}{dt}\right)_{t\to 0} = \beta J \tag{15}$$

Under perfect sink boundary conditions, which can exist when the adsorbate has a high affinity for the sorbent surface, this probability equals one [19]. This will likely be the case for adsorption of neutral polymers such as PEG [1]. As a consequence, in these systems, the initial rate of adsorption should be equal to the maximum rate of mass transfer from the bulk (J) [1].

3. Results and discussion

In order to demonstrate that the experimental setup presented in this study enables the formation of a stagnation point and that the adsorption process can be described by Eq. (14), two different approaches (one theoretical and one experimental) were taken. The results of each strategy are herein discussed and compared. Subsequently, a methodology to correct the obtained kinetic parameters to account for the size of the measured spot is proposed.

3.1. Computational fluid dynamics

Initially, the development of the flow fields in the cell was investigated. Fig. 2 shows the velocity profiles for Re of 2.8, 12.0, 24.7, and 49.2. The streamlines can be interpreted as the path of fluid on the cell so the line tangent to the streamline represents the direction of the fluid velocity vector at a given point in space [40]. As can be observed in Fig. 2, characteristic hyperbolic field lines around the point where the flow intersects with the substrate are developed, supporting the presence of a stagnation point. It is also noted that the streamlines slightly deviate from hyperbolas at high Re. This behavior observed at high Re leads to a vortex formation away from the stagnation point. However, its presence should not affect the adsorption process because it is relatively far from the interface. Similar flow patterns have been previously reported in the literature for other impinging-jet geometries [10,40,61].

As noted by Dabros and van der Ven [10], the main advantage of performing adsorption experiments under stagnation point conditions is that the influence of hydrodynamic disturbances on the flow near the stagnation point can be eliminated. Although it has

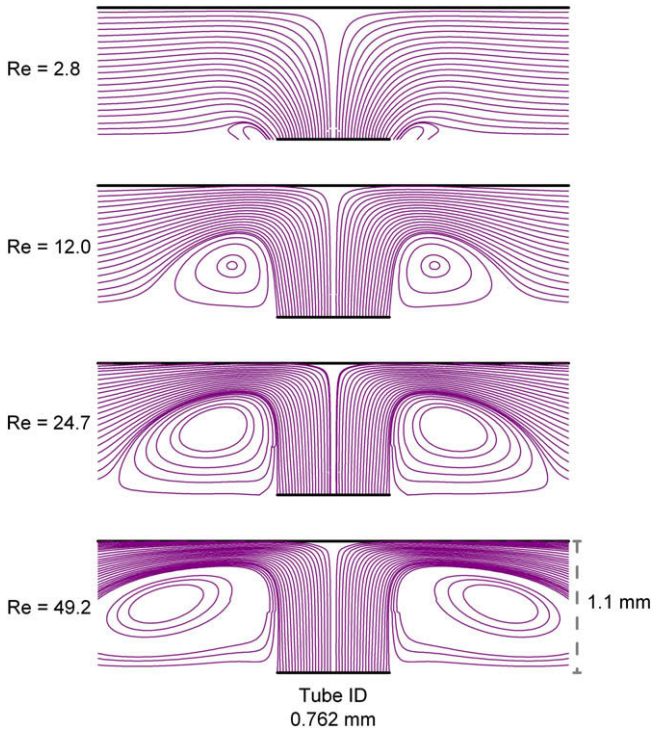

Fig. 2. Fluid streamlines from the inlet tube to the substrate determined by computational fluids dynamics for Reynolds numbers used in this study. In all cases $h/R = 2.8$.

been generally reported that α is roughly proportional to Re [1,10], no information was available for the specific setting of our cell design ($h/R = 2.8$). Consequently, to demonstrate that the described cell allows the development of stagnation flow conditions, the dependence of the dimensionless parameter α with respect to Re was calculated (see Fig. 3) for two different cell designs featuring $h/R = 2.8$ and $h/R = 5$ and compared to previously reported data for $h/R = 1$ and $h/R = 1.7$ [10]. As can be observed, the model herein described follows the same general trend that others previously reported. Although designs with large h/R values suffer from low mass-transfer efficiencies [62], the value selected for our cell lays in the range of 1.5–4, which is considered optimum for adsorption kinetic measurements [10]. More details regarding the characterization of cells with other geometries can be found elsewhere [1,10,62,63].

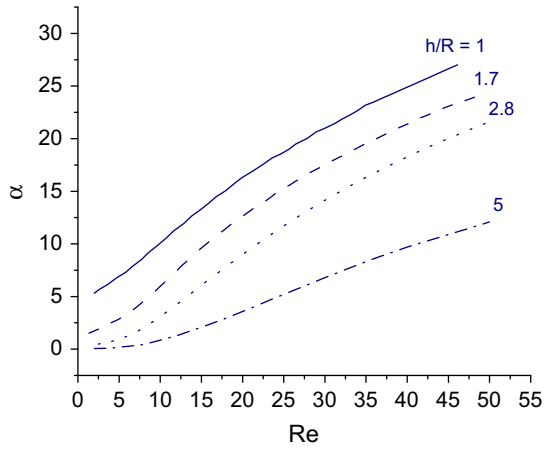

Fig. 3. Dependence of the flow intensity parameter (α) on the Reynolds number (Re) for several values of h/R. The data for $h/R = 1$ and 1.7 was used with permission from Ref. [10].

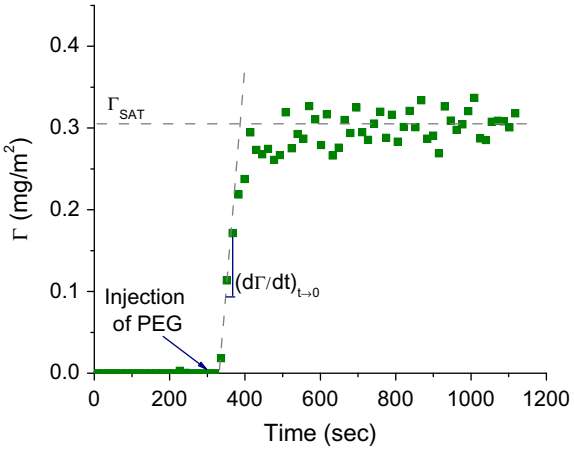

Fig. 4. Example of a typical curve for adsorption of PEG onto Si/SiO_2 substrate. Conditions: $M_w = 93{,}000$ g mol^{-1}, concentration 3 mg L^{-1} and Re = 24.7.

3.2. Adsorption of PEG

It is well-known that PEG readily adsorbs to a variety of materials with high affinity and with no significant energy barriers [9,64,65]. Therefore, the adsorption of PEG is determined by the mass transfer rate from the bulk solution, making it reasonable to assume $\beta = 1$ [1]. Consequently, the initial adsorption rate ($(d\Gamma/dt)_{t\to 0}$) of PEG (as measured in our cell) should be equal to the flux (J) of PEG to the surface, following Eq. (14).

A typical dynamic adsorption experiment is shown in Fig. 4. In agreement with previous reports [1,59,66], an initial fast adsorption process, followed by a slower one was always observed. Dynamic measurements (see Fig. 4) enabled calculating the initial adsorption rate ($(d\Gamma/dt)_{t\to 0}$) under different experimental conditions. The results are summarized in Fig. 5.

As can be observed in Fig. 5A, the initial rate of adsorption of PEG was proportional to the concentration of polymer in the impinging jet. Fig. 5B shows that a linear dependence between the initial adsorption rate and $D^{2/3}$ was obtained when polymers with different molecular weights (~8000–280,000 g mol^{-1}) were adsorbed ($c = 1$ mg L^{-1}). Γ_{SAT} values of 0.16 ± 0.02 mg m^{-2}, 0.33 ± 0.02 mg m^{-2}, and 0.40 ± 0.05 mg m^{-2} were obtained for PEG with molecular weights of 8730, 93,000, and 278,100 g mol^{-1}, respectively. These results follow the general theory behind polymer adsorption which predicts an increase in Γ_{SAT} for larger adsorbing molecules [1,16]. Furthermore, as shown in Fig. 5C, $(d\Gamma/dt)_{t\to 0}$ increases with an increase in $Re^{1/3}$ in the concentration range (0.5–5 mg L^{-1}) studied.

In general, the initial adsorption rates obtained for our system were smaller than those previously reported with different cell setups (same polymer and $h/R = 1.6$) [1]. This can be in part explained by the difference in h/R value. The higher h/R value selected for our cell implies a lower α (see Fig. 3) and, consequently, a lower rate of mass transfer. Furthermore, despite the fact that the experimental data obtained with our system followed the trends predicted by Eq. (14), the initial adsorption rates were significantly lower than the flux of PEG towards the surface at the stagnation point (as predicted by Eq. (14)). It is necessary to note that the ellipsometer, as many other optical techniques, acquires data over a relatively large area compared to the infinitesimal stagnation point. In fact, it has been previously reported [19] that initial adsorption rates obtained by reflectometry (under stagnation point flow conditions

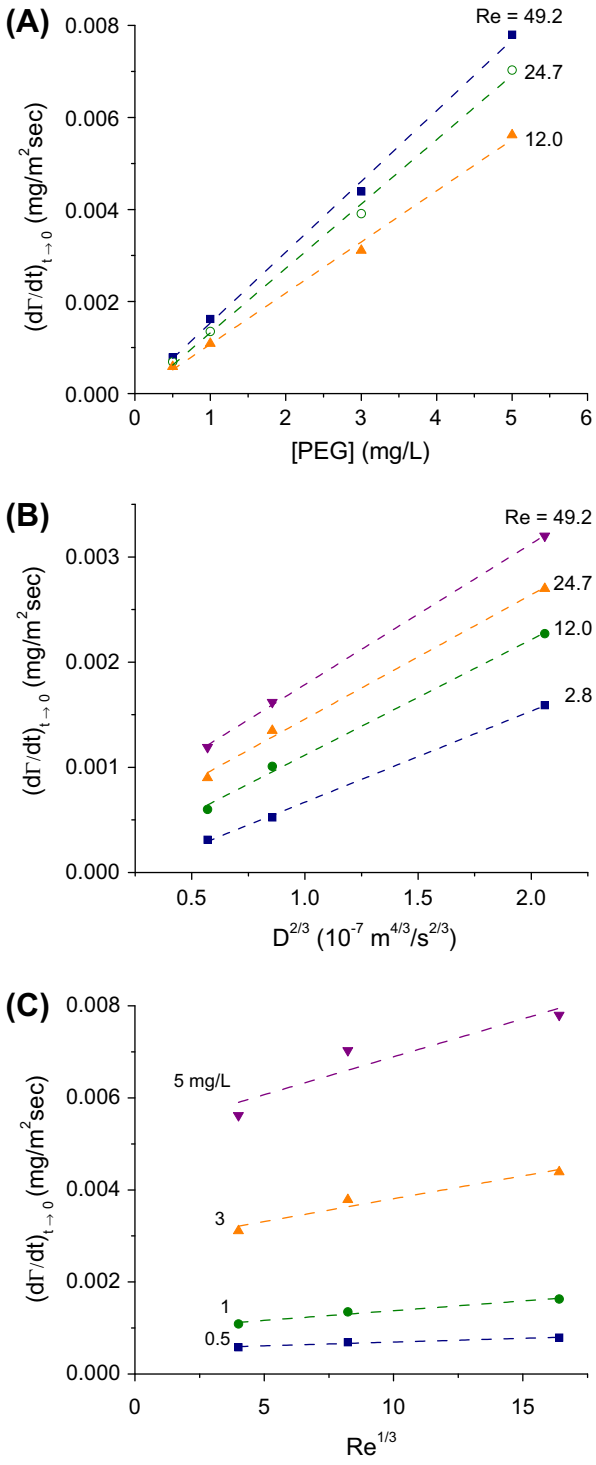

Fig. 5. Initial adsorption rate of PEG as a function of: (A) the concentration for three Re numbers (93,000 g mol^{-1}), (B) the diffusion coefficient (c = 1 mg L^{-1}), and (C) the cube root of the Reynolds number for different PEG concentrations (M_w = 93,000 g mol^{-1}).

and for transport limited adsorption processes) are only 50–80% of the theoretical values predicted by Eq. (14). Because the local mass flux decreases significantly at interfacial points away from the stagnation point, the *average* mass transfer, i.e. measured mass transfer, to the substrate decreases with increasing the area of measurement (compared to the stagnation point) [19]. Theoretical calculations performed by Adamczyk et al. [67] using a circular spot rather than a point, demonstrated that the measurement over an area rather than at a point is indeed the source of deviation of experimental values from the theoretical ones for the stagnation point. In fact, it was shown that when the radius of the measured spot (r) equals to the radius of the inlet tube (r/R = 1), the experimentally obtained adsorption rates are only 90% and 70% of the flux at the stagnation point for Re of 1 and 48, respectively. The mentioned underestimation of the initial adsorption rates should be accounted for in our system because the area of the measured spot is significantly larger (approximately 7 mm^2) than the values normally reported in the literature for reflectometry (~1 mm^2). In fact, it was determined by computational dynamics that for our experimental setup, α reaches a value of approximately zero when the distance from the stagnation point (r) is greater than three times the radius of the impinging tube (see Supplementary information). It should be considered here that the estimated area of the measured spot in our ellipsometer comprises interfacial points that yield $r/R > 3$ where α is actually very low. It is also worth noting that because α depends on Re, the errors in the experimental data are also Re-dependent for a fixed area around the stagnation point [67]. This fact complicates the comparison of the results obtained for different Re numbers even within the same experimental setup and, in turn, highlights the necessity of finding a setup-specific correction function. Such function would allow researchers to reasonably estimate the adsorption kinetics at the stagnation point and quantitatively compare their results even when using different cell setups and techniques.

In order to find such a function, the experimental initial adsorption rates ($(d\Gamma/dt)_{t\to 0}$) were analyzed in relation to the theoretical values for flux predicted by Eq. (14) (J_{THEO}). It was observed (see Supplementary information) that, in agreement with previous reports from the literature [67], the correction needed to account for the size of the measured spot is a function of Re. Subsequently, the ratio $J_{THEO}/(d\Gamma/dt)_{t\to 0}$ was assumed to be a simple power function of Re and a correction function was empirically obtained (Eq. (16)).

$$J_{THEO} \approx \left(\frac{d\Gamma}{dt}\right)_{Corrected} = \left(\frac{d\Gamma}{dt}\right)_{t\to 0} \times 2.3406 \times Re^{0.4094} \qquad (16)$$

The corrected initial adsorption rates ($(d\Gamma/dt)_{Corrected}$) provide a more realistic estimation of the adsorption kinetics at the stagnation point. It is worth noting that only experiments performed

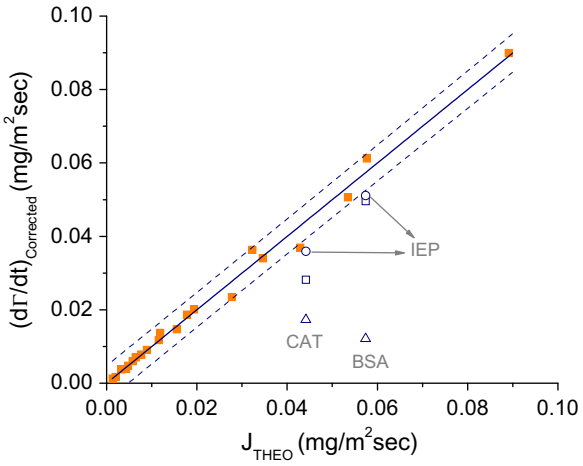

Fig. 6. Corrected experimental values ($(d\Gamma/dt)_{Corrected}$) calculated from Eq. (16) versus the theoretical flux (J_{THEO}) calculated from Eq. (14) for PEG. All of the experiments were included. The solid line represents the linear fit (slope = 1.00 ± 0.02, R^2 = 0.9948). Dashed lines represent the prediction bands for a 95% confidence level. $(d\Gamma/dt)_{Corrected}$ for catalase (CAT) and bovine serum albumin (BSA) below (□), at (○), and above (△) the IEP (c = 0.005 mg mL^{-1}).

using adsorbates with well-known behavior (such as PEG, $(d\Gamma/dt)_{t\to 0} = J$) would allow the calculation of this function for a given set of experimental conditions. Fig. 6 shows the correlation between experimental values after applying the correction function ($(d\Gamma/dt)_{\text{Corrected}}$) and the theoretical initial adsorption rates (J_{THEO}). As can be observed, a very good agreement between the two parameters was obtained (slope = 1.00 ± 0.02, $R^2 = 0.9948$) indicating that the correction is valid for all data points. It is also worth mentioning that this function would only be valid for the experimental setup described in this paper. Any other cell with a specific geometry (h/R) and size of the measuring spot will generate data with different ratios and consequently, another expression of the correction function will be necessary.

In order to verify the applicability of the correction function to other analytes, the adsorption of two proteins (catalase and bovine serum albumin) with different molecular weights was studied (see Table 1). For these proteins, the initial adsorption rates obtained at pH values above, at, and below the isoelectric point were measured and corrected using Eq. (16). It is well-known that proteins exhibit different adsorption behavior depending on the pH of the solution because their net charge (and therewith the attachment probability) is affected by the pH [43,68–70]. When the adsorbing analyte and the surface are both neutral or have opposite charges, there are no electrostatic barriers for the adsorption and, therefore, the initial adsorption rate should be larger than in the case when similar charges are present. In the latter case, the energy barrier is produced by the repulsion between the adsorbate and the sorbent surface. Accordingly, the $(d\Gamma/dt)_{\text{Corrected}}$ for both proteins at the IEP fall close to the 95% confidence interval predicted by Eq. (16) (see Fig. 6), resembling the adsorption rates obtained for PEG. These results suggest that under these conditions, the efficiency factor (β) is close to one. These results can be explained by considering that at the IEP, proteins do not have a net charge and therefore the electrostatic repulsion between the molecules and the surface is minimal. On the other hand, the $(d\Gamma/dt)_{\text{Corrected}}$ obtained above the IEP was smaller than at the corresponding IEP likely due to electrostatic repulsion between the protein and the surface. Under these conditions, the adsorption rate after correction $(d\Gamma/dt)_{\text{Corrected}}$ is much smaller than the J_{THEO} indicating a reduction in the efficiency factor ($\beta \ll 1$). At pH values below the IEP the results were different for the two proteins. For BSA, when the protein is positively charged, the initial adsorption rate is similar to the one obtained at the IEP because there is an attraction between the protein and the surface, so there is no barrier for the adsorption. These results are in agreement with previous reports [69,71]. For catalase, at low pH values the $(d\Gamma/dt)_{\text{Corrected}}$ was smaller than the corresponding adsorption rate at the IEP. This result can be due to electrostatic repulsion between the protein molecules due to their high positive charge which also reduces the attachment efficiency. Similar results have been reported for other proteins on different surfaces [70,72].

It is evident from the results discussed here that the correction of the initial adsorption rates with the function obtained from PEG provides reasonable results. Thus, the correction function depends only on the cell setup and the instrumentation used, and does not depend specifically on the adsorbate/substrate under study.

4. Conclusions

The paper describes a simple modification to a commercial cell that enables the investigation of adsorption processes under stagnation point flow conditions using spectroscopic ellipsometry. Theoretical calculations executed by computational fluid dynamics as well as adsorption experiments performed with PEG on SiO_2 support the existence of stagnation point flow in the cell design described in this paper. In all cases, these results are consistent with previous reports stating that the adsorption of PEG to silica surfaces can be considered a fast process controlled by the transport of the adsorbate to the surface, rather than the transfer from the subsurface to the interface [73]. In addition, the use of a setup-specific correction function that should be determined and applied to the experimental data in order to correct for the size of the measuring spot and for variations in mass transfer away from the stagnation point was proposed. This correction should allow quantitative comparisons of results obtained by different research groups using various techniques and experimental conditions. The validity of the correction function for other adsorbates was also demonstrated. In addition, the application of the mentioned correction allowed to distinguish between situations where $\beta \approx 1$ and where $\beta \ll 1$.

Acknowledgments

Financial support for this project was provided in part by The University of Texas at San Antonio, and the National Institute of General Medical Sciences (NIGMS)/National Institutes of Health (1SC3GM081085).

Appendix A. Supplementary material

Supplementary data associated with this article can be found, in the online version, at doi:10.1016/j.jcis.2010.02.019.

References

[1] J.C. Dijt, M.A. Cohen Stuart, J.E. Hofman, G.J. Fleer, Colloid Surf. A 51 (1990) 141.
[2] Y. Lvov, K. Ariga, I. Ichinose, T. Kunitake, Thin Solid Films 284–285 (1996) 797.
[3] D.F. Siqueira, J. Reiter, U. Breiner, R. Stadler, M. Stamm, Langmuir 12 (1996) 972.
[4] Y. Wang, P.L. Dubin, Anal. Chem. 71 (1999) 3463.
[5] M.A. Cohen Stuart, A. de Keizer, in: J. Wingrave (Ed.), Marcel Dekker, New York, 2001, pp. 157–199.
[6] A. Laguecir, S. Stoll, Polymer 46 (2005) 1359.
[7] P. Liu, Appl. Clay Sci. 38 (2007) 64.
[8] C.C. Buron, C. Filiâtre, F. Membrey, C. Bainier, D. Charraut, A. Foissy, Colloid Surf. A 305 (2007) 105.
[9] C.Y. Chang, W.T. Tsai, C.H. Ing, C.F. Chang, J. Colloid Interface Sci. 260 (2003) 273.
[10] T. Dabros, T.G.M. Van de Ven, Colloid Polym. Sci. 261 (1983) 694.
[11] C. Yang, T. Dabros, D. Li, J. Czarnecki, J.H. Masliyah, J. Colloid Interface Sci. 208 (1998) 226.
[12] R.S. Sanders, R.S. Chow, J.H. Masliyah, J. Colloid Interface Sci. 174 (1995) 230.
[13] A.I. Abdel-Fattah, M.S. El-Genk, P.W. Reimus, J. Colloid Interface Sci. 246 (2002) 241.
[14] J.M. Meinders, J. Noordmans, H.J. Busscher, J. Colloid Interface Sci. 152 (1992) 265.
[15] T. Tjärnhage, G. Puu, Colloid Surf. B 8 (1996) 39.
[16] N.L. Filippova, J. Colloid Interface Sci. 211 (1999) 336.
[17] L. Wagberg, I. Nygren, Colloid Surf. A 159 (1999) 3.
[18] B. Yuan, M. Pham, T.H. Nguyen, Environ. Sci. Technol. 42 (2008) 7628.
[19] M.R. Böhmer, E.A. van der Zeeuw, G.J.M. Koper, J Colloid Interface Sci 197 (1998) 242.
[20] L.-E. Enarsson, L. Wågberg, Langmuir 24 (2008) 7329.
[21] J.C. Dijt, M.A.C. Stuart, G.J. Fleer, Adv. Colloid Interface Sci. 50 (1994) 79.
[22] G. García, C.D. García, P.I. Ortiz, C.P. De Pauli, J. Electroanal. Chem. 519 (2002) 53.
[23] R. Atkin, V.S. Craig, E.J. Wanless, S. Biggs, J. Colloid Interface Sci. 266 (2003) 236.
[24] Z. Adamczyk, B. Siwek, M. Zembala, P. Weronski, Langmuir 8 (1992).
[25] M. Polverari, T.G.M. Van de Ven, J. Colloid Interface Sci. 173 (1995) 343.
[26] W.M. de Vos, P.M. Biesheuvel, A. de Keizer, J.M. Kleijn, M.A. Cohen Stuart, Langmuir 24 (2008) 6575.
[27] B.D. Riquelme, J.R. Valverde, R.J. Rasia, Optic. Laser Eng. 39 (2003) 589.
[28] H. Fujiwara, Spectroscopic Ellipsometry. Principles and Applications, J. Wiley&Sons, West sussex, England, 2007.
[29] H. Elwing, Biomaterials 19 (1998) 397.
[30] F. Hook, B. Kasemo, T. Nylander, C. Fant, K. Sott, H. Elwing, Anal. Chem. 73 (2001) 5796.
[31] J.L. Wehmeyer, R. Synowicki, R. Bizios, C.D. García, Mater. Sci. Eng. B 30 (2010) 277.
[32] L.L. Foose, H.W. Blanch, C.J. Radke, Langmuir 24 (2008) 7388.
[33] M. Poksinski, H. Arwin, Thin Solid Films 455–456 (2004) 716.

[34] S. Lousinian, S. Logothetidis, Microelectron. Eng. 84 (2007) 479.
[35] A. Tsargorodskaya, A.V. Nabok, A.K. Ray, Nanotechnology (2004) 703.
[36] M.J. Avena, L.K. Koopal, Environ. Sci. Technol. 33 (1999) 2739.
[37] H. Arwin, Thin Solid Films 313 (1998) 764.
[38] A.F. Naves, A.M. Carmona-Ribeiro, D.F.S. Petri, Langmuir 23 (2007) 1981.
[39] M.A. Pérez, M. López Teijelo, Thin Solid Films 449 (2004) 138.
[40] Z. Adamczyk, J. Colloid Interface Sci. 229 (2001) 477.
[41] P.J.A. Kenis, R.F. Ismagilov, S. Takayama, G.M. Whitesides, S. Li, H.S. White, Acc. Chem. Res. 33 (2000) 841.
[42] D.J. Tritton, Physical Fluid Dynamics, 2nd ed., Oxford University Press, New York, 1988.
[43] J. Buijs, P.A.W. Van den Berg, J.W.T. Lichtenbelt, W. Norde, J. Lyklema, J. Colloid Interface Sci. 178 (1996) 594.
[44] T. Samejima, M. Kamata, K. Shibata, J. Biochem. 51 (1962) 181.
[45] C.E. Giacomelli, M.J. Avena, C.P. De Pauli, J. Colloid Interface Sci. 188 (1997) 387.
[46] R.H. Boyd, P.J. Phillips, The Science of Polymer Molecules, Cambridge University Press, New York, NY, 1996.
[47] J. Shao, R.E. Baltus, AIChE J. 46 (2000) 1149.
[48] M. Vinnichenko, R. Gago, N. Huang, Y.X. Leng, H. Sun, U. Kreissig, M.P. Kulish, M.F. Maitz, Thin Solid Films 455–456 (2004) 530.
[49] L.M. Karlsson, M. Schubert, N. Ashkenov, H. Arwin, Thin Solid Films 455–456 (2004) 726.
[50] X. Wang, Y. Wang, H. Xu, H. Shan, J.R. Lu, J. Colloid Interface Sci. 323 (2008) 18.
[51] S. Lousinian, S. Logothetidis, A. Laskarakis, M. Gioti, Biomol. Eng. 24 (2007) 107.
[52] H. Arwin, Thin Solid Films 377–378 (2000) 48.
[53] J. Wen, T. Arakawa, Anal. Biochem. 280 (2000) 327.
[54] J. Benesch, A. Askendal, P. Tengvall, Colloids Surf. B 18 (2000) 71.
[55] J.A. De Feijter, J. Benjamins, F.A. Veer, Biopolymers 17 (1978) 1759.
[56] B.A. Noskov, A.V. Akentiev, D.O. Grigoriev, G. Loglio, R. Miller, J. Colloid Interface Sci. 282 (2005) 38.
[57] S.J. McClellan, E.I. Franses, Colloid Surf. B 28 (2003) 63.
[58] H.A. Sober, Handbook of Biochemistry: Selected Data for Molecular Biology, Chem. Rubber Co., Cleveland, Ohio, 1968. p. 982.
[59] J.C. Dijt, M.A.C. Stuart, G.J. Fleer, Macromolecules 27 (1994) 3207.
[60] M.C.P. van Eijk, M.A. Cohen Stuart, Langmuir 13 (1997) 5447.
[61] Z. Adamczyk, L. Szyk, P. Warszynski, J. Colloid Interface Sci. 209 (1999).
[62] Z. Adamczyk, in: Particles at Interfaces: Interactions, Deposition, Structure, Academic Press, London, UK, 2006 (vol. 9).
[63] A.J. de Kerchove, P. Weronski, M. Elimelech, Langmuir 23 (2007) 12301.
[64] N. Derkaoui, S. Said, Y. Grohens, R. Olier, M. Privat, Langmuir 23 (2007) 6631.
[65] B. Zdyrko, P.B.-Y. Ofir, A.M. Alb, W.F. Reed, M.M. Santore, J. Colloid Interface Sci. 322 (2008) 365.
[66] S.K. Parida, S. Dash, S. Patel, B.K. Mishra, Adv. Colloid Interface Sci. 121 (2006) 77.
[67] Z. Adamczyk, B. Siwek, P. Warszynski, E. Musial, J. Colloid Interface Sci. 242 (2001) 14.
[68] T. Arai, W. Norde, Colloid Surf 51 (1990) 1.
[69] M.G.E.G. Bremer, J. Duval, W. Norde, J. Lyklema, Colloid Surf. A 250 (2004) 29.
[70] M. van der Veen, W. Norde, M.C. Stuart, Colloid Surf. B 35 (2004) 33.
[71] L.E. Valenti, P.A. Fiorito, C.D. Garcia, C.E. Giacomelli, J. Colloid Interface Sci. 307 (2007) 349.
[72] M.F. Mora, C. Giacomelli, C. Garcia, Anal. Chem. 81 (2009) 1016.
[73] A.M. Díez-Pascual, A. Compostizo, A. Crespo-Colín, R.G. Rubio, R. Miller, J. Colloid Interface Sci. 307 (2007) 398.
[74] L. He, B. Niemeyer, Biotechnol. Progr. 19 (2003) 544.